Electrical properties of GaN-based MIS-structures with Al_2O_3 deposited by ALD using both water and ozone as the oxygen precursors

Toshiharu Kubo, Joseph J. Freedsman, Yasuhiro Iwata, and Takashi Egawa

Research Center for Nano-Device and System, Nagoya Institute of Technology, Nagoya 466-8555, Japan

Al_2O_3 deposited by atomic layer deposition (ALD) was focused as an insulator in metal-insulator-semiconductor (MIS) structures for GaN-based MIS-devices. As the oxygen precursors for the ALD process, water (H_2O), ozone (O_3), and both H_2O and O_3 were used. The chemical characteristics of the ALD-Al_2O_3 surfaces were investigated by an X-ray photoelectron spectroscopy (XPS). After fabrication of MIS-diodes and MIS-high-electron-mobility transistors (MIS-HEMTs) with the ALD-Al_2O_3, their electrical properties were evaluated by current-voltage (*I*-*V*) and capacitance-voltage (*C*-*V*) measurements. The threshold voltage of the *C*-*V* curves for MIS-diodes indicate that the fixed charge in the Al_2O_3 layer is decreased by using both H_2O and O_3 as the oxygen precursors. Furthermore, MIS-HEMTs with the H_2O+O_3-based Al_2O_3 showed the good DC *I*-*V* characteristics with the forward bias over 6 V, and the drain leakage current in the off-state region was suppressed by seven orders of magnitude.

E-mail address: kubo.toshiharu@nitech.ac.jp

1. Introduction

AlGaN/GaN high-eletron-mobility transistors (HEMTs) with the metal-insulator-semiconductor (MIS) structure are expected to be used for the next generation high-power and high-frequency switching device applications. The MIS-structure is effective for the gate leakage reduction and the large gate voltage swing. As an insulator for the MIS-structure, a lot of materials, such as Al_2O_3,[1-11] HfO_2,[10,12,13] SiO_2,[1,14-16] AlN,[17-21] and SiN,[1,22-25] have been studied. Among such insulators, Al_2O_3 is a promising material due to its relatively large band gap and high dielectric constant, and MIS-HEMTs with Al_2O_3 have been fabricated by several deposition methods, for example, oxidation of Al layer[1,4,5,9] and atomic layer deposition (ALD).[2,3,6,7,8,10,11]

In this study, ALD was focused as the deposition method of Al_2O_3. The ALD can offer the oxide layer which is pinhole free and uniform in thickness. In the ALD process, water (H_2O) is often used as the oxygen precursor. However, it has been reported that impurities in oxides deposited by ALD on Si can be reduced by using ozone (O_3) instead of H_2O.[26-29] It is considered that the hydroxyl group (-OH) as an impurity in oxides can be reduced by using O_3 instead of H_2O. In the ALD process using H_2O, the introduction of H_2O after the introduction of trimethylaluminum (TMA) causes some reactions, such as $-CH_3 + H_2O \rightarrow -OH + CH_4$, and the surface is covered by the -OH, while the surface is covered by O in the ALD process using O_3 with the reaction, such as $-6CH_3 + 2O_3 \rightarrow -6O + 3C_2H_6$. On the other hand, it is considered that the carbon (C) content in oxides is increased by using O_3.[27] The high reactivity of O_3 generates many carbonates by the reaction, such as $-CH_3 + O_3 \rightarrow CO_2 + H_2 + -OH$. Therefore, both H and C contents can be reduced by using both H_2O and O_3, namely the introduction of O_3 after the introduction of H_2O. The main effect of the O_3 pulse following the H_2O pulse is considered to cut O-H bonds and remove the -OH .

In this study, Al_2O_3 films on GaN and the GaN-based MIS-diodes and MIS-HEMTs with

Al_2O_3 were fabricated by ALD using H_2O, O_3, and both H_2O and O_3, and their chemical and electrical properties were investigated.

2. Deposition and characterization of ALD-Al_2O_3

First, to investigate the chemical characteristics of the ALD-Al_2O_3 films, 20-nm-thick Al_2O_3 layers were deposited on GaN at 250^{o}C and 300^{o}C by using Cambridge Nanotech ALD system. H_2O, O_3, and both H_2O and O_3 were used as the oxygen precursors, and TMA was used as the aluminum precursor, which were used as the precursors for ALD-Al_2O_3 in this study. Figure 1 shows the schematic diagram of the ALD process using both H_2O and O_3. The ALD processes using H_2O or O_3 were similar to the process shown in Fig. 1. The thicknesses of Al_2O_3 layers were confirmed by an elliprometer and transmission electron microscopy (TEM) images.

The chemical characteristics of the ALD-Al_2O_3 surfaces were investigated by an X-ray photoelectron spectroscopy (XPS; PHI Quantera SXM) equipped with a monochromated Al Kα radiation source (hν = 1486.6 eV). The electron-escape angle in this study was 45^o. Figures 2(a) and (b) show Al 2p and O 1s core-level spectra obtained from the ALD-Al_2O_3 surfaces deposited at 300^{o}C. The deposition temperature dependence of the XPS spectra was within the measurement error range. The peak position of the Al 2p level was consistent with that of the aluminum oxide regardless of the oxide precursor, while the full width at half maximum (FWHM) of the Al 2p spectrum obtained from the H_2O-based Al_2O_3 surface was wider than those obtained from the O_3-based and the H_2O+O_3-based Al_2O_3 surfaces. These results indicate that at least Al-Al metallic bonding can be reduced by using O_3 or H_2O+O_3 instead of H_2O. Kim et al. also reported similar effect in ref. 4. The band gap energy (E_g) of ALD-Al_2O_3 was estimated from the O 1*s* spectra shown in Fig. 2(b). The spectrum of the O 1s level was shifted to lower energy by 1.2 eV in order to check the E_g easily, and all spectra

did not depend on the oxygen precursor within the measurement error range. The E_g was approximately 6.6 eV in all cases of H_2O, O_3, and H_2O+O_3-based Al_2O_3, which is the usual value for the Al_2O_3 film deposited using the H_2O-based ALD.[11]

The amount of impurities in the ALD-Al_2O_3 was investigated by secondary ion mass spectroscopy (SIMS). Table I shows the concentrations of H and C contents at a depth of 10 nm from the surface of ALD-Al_2O_3 deposited at 300^{o}C. As expected, the H content was decreased, and the C content was increased by using O_3 instead of H_2O. On the other hand, by using both H_2O and O_3, both the H and C contents were decreased compared to those in the H_2O-based Al_2O_3, while the H content was higher than that in the O_3-based Al_2O_3. The amount of the H content showed the expected behavior. The possible reason why the C content in the H_2O+O_3-based Al_2O_3 was less than that in the H_2O-based Al_2O_3 is that the residual carbon compounds after introducing H_2O were released by the reaction with O_3. The decrease of both the H and C contents in the H_2O+O_3-based Al_2O_3 was considered to be preferable for the GaN-based MIS-devices.

3. Fabrication and measurement of MIS-diodes

In order to investigate the *I-V* and *C-V* characteristics of the MIS-diodes with ALD-Al_2O_3, the Al_2O_3/n-GaN MIS-diodes were fabricated. The epitaxial Si-doped GaN films were grown on sapphire substrates using a Taiyo Nippon Sanso SR-4000 metal organic chemical vapor deposition (MOCVD) system. The donor concentration was 1.5×10^{16} cm^{-3}, which was estimated from the *C-V* measurement on Schottky contacts. 20-nm-thick Al_2O_3 layers were deposited by ALD at 250^{o}C and 300^{o}C with pretreatment in HCl solution. Using conventional lithography, ring-shaped ohmic contacts (Ti/Al/Ni/Au: 15/80/12/40) were fabricated onto the n-GaN surface as cathodes and annealed at 775^{o}C for 30 s in N_2 atmosphere. Finally, circular-shaped metals (Pd/Ni/Au: 40/20/60 nm) were deposited as anodes inside the

ring-shaped cathodes. The anode diameter was 200 μm. The schematic cross section view of the Al_2O_3/n-GaN MIS-diode is shown in Fig. 3. For comparison, Schottky-type diodes were also fabricated in the same way as the MIS-diodes. After fabricating the diodes, *I-V* and *C-V* measurements were carried out at room temperature in the dark using an Agilent B1505A power device analyzer. The frequency of *C-V* measurements was 100 kHz.

Figures 4(a), (b) and (c) show the typical results of *I-V* measurements. The result of the Schottky-diode is also shown in Fig. 4(c). As shown in Figs. 4, the leakage current of the MIS-diodes was suppressed compared to that of the Schottky-diode, and the current through the H_2O-based Al_2O_3 was decreased with increasing the deposition temperature (T_d) from 250^{o}C to 300^{o}C, while the current thorough the O_3-based Al_2O_3 was increased with increasing the T_d. These results seem to suggest that impurities related to the leakage current such as -OH in the H_2O-based Al_2O_3 were decreased with increasing the T_d by the higher reaction rate between -OH and -CH_3, while such impurities in the O_3-based Al_2O_3 were increased with increasing the T_d by the increasing reaction rate between -CH_3 and O_3. The current through H_2O+O_3-based Al_2O_3 seems to show the intermediate behavior between those of the H_2O-based and the O_3-based Al_2O_3. The leakage current through Al_2O_3 deposited by ALD using O_3 was more stable for the T_d distribution than that through the H_2O-based Al_2O_3.

The typical results of *C-V* measurements for Al_2O_3/n-GaN MIS-diodes are shown in Fig. 5(a), (b) and (c). The dielectric constant (ε) of the H_2O-based Al_2O_3 was approximately 9.5, and that of the O_3-based and the H_2O+O_3-based Al_2O_3 was approximately 8.5, which was calculated from the expression: $C = \varepsilon S / d$, where S is the area of the anode and d is the thickness of the Al_2O_3. These values of ε were usual values for Al_2O_3. As shown in Fig. 5(a), the threshold voltage (V_{th}) was defined as the point where the extrapolated line of the *C-V* curve crosses the horizontal axis. It was found that V_{th} shifted in the positive direction in all cases of oxygen precursors with increasing the T_d from 250^{o}C to 300^{o}C. This result suggests

that the fixed charge in the ALD-Al_2O_3 is decreased with increasing the T_d. Table II shows the V_{th} of the *C-V* curve obtained from the MIS-diodes with Al_2O_3 deposited at 300°C. The V_{th} with Al_2O_3 deposited using both H_2O and O_3 was the closest to the ideal one whose *C-V* curve is shown in Fig. 5(c), which implies that the fixed charge in ALD-Al_2O_3 was most reduced by using both H_2O and O_3. Furthermore, the V_{th} of the MIS-diode with the H_2O+O_3-based Al_2O_3 was the most stable for the T_d distribution compared to those through the H_2O-based and the O_3-based Al_2O_3.

5. Fabrication and measurement of MIS-HEMTs

The AlGaN/GaN heterostructures were grown on 4-in. p-type Si (111) substrates by the MOCVD system. The grown structure consists of 25 nm $Al_{0.26}GaN$ layer, 1 μm GaN layer, and 2.5 μm buffer layer on 4-in. p-type Si (111) substrate.

The device process started with a mesa isolation by BCl_3 plasma based reactive ion etching. Using conventional lithography, source/drain ohmic contacts (Ti/Al/Ni/Au: 15/80/12/40 nm) were made onto the devices and annealed at 850°C for 30 s while flowing nitrogen gas. 20-nm-thick Al_2O_3 layers were deposited by ALD at 300°C with pretreatment in HCl solution. After the gate lithography, Pd/Ni/Au (40/20/60 nm) was deposited as the gate contact. The schematic cross section view of the MIS-HEMT is shown in Fig. 6. The dimensions of the fabricated HEMTs were as follows: source-gate spacing (L_{sg}) = 4 μm, gate width (W_g) = 200 μm, gate length (L_g) = 2 μm, and gate-drain spacing (L_{gd}) = 4 μm. For comparison, the Schottky gate HEMTs were also fabricated in the same way as the MIS-HEMTs. In order to investigate the electrical properties, the drain current-voltage (I_d-V_d) characteristics were measured using an Agilent B1505A power device analyzer.

Figure 7(a) shows the DC I_d-V_d characteristics of the MIS-HEMT with the H_2O+O_3-based Al_2O_3. As shown in Fig. 7(a), the good pinch-off characteristics was obtained. The maximum

I_d was 420 mA/mm at a gate voltage of 7 V, and the maximum g_m was 80 mS/mm. Furthermore, the V_{th} shift of the MIS-HEMT to the positive direction was observed. One of the reasons of the V_{th} shift might be the electron trap at the gate region. As for the MIS-HEMTs with the H_2O-based and the O_3-based Al_2O_3, the typical example of the DC I_d-V_d characteristics is shown in Fig. 7(b). As shown in Fig. 7(b), they did not show the pinch-off characteristics. This result seems to be caused by the high interface state and the trap state density due to impurities, such as -OH and carbonates introduced during the ALD process. Figure 8 shows the dependence of the I_d and the gate leakage current (I_g) on the gate bias voltage (V_g). The off-state region indicates that the I_g was suppressed by the MIS-structure from 10^{-2} mA/mm to 10^{-9} mA/mm, which was the measurement limit. Moreover, the forward bias over 6 V could be applied to the MIS-HEMT. In order to reduce the -OH in Al_2O_3 deposited by ALD and improve the *I-V* characteristics of MIS-HEMT$_S$, the post deposition annealing (PDA) above 700^{o}C is effective.[30] However, it was reported that such high temperature annealing generates microcrystallization regions in the ALD-Al_2O_3, whose grain boundaries can serve as high-leakage paths.[8] On the other hand, by using both H_2O and O_3, the MIS-HEMT shows the good *I-V* characteristics without the PDA. Therefore, the I_g through the H_2O+O_3-based Al_2O_3 can be lower than the I_g through the H_2O-based and the O_3-based Al_2O_3. These results obtained from the MIS-HEMTs indicate that the Al_2O_3 deposited by ALD using both H_2O and O_3 as the oxygen precursors is useful for fabricating GaN-based MIS-devices.

6. Conclusions

Al_2O_3 was deposited by ALD on GaN using H_2O, O_3, and both H_2O and O_3 as the oxygen precursors. XPS results indicate that Al-Al metallic bonding in the ALD-Al_2O_3 can be reduced by using O_3 or both H_2O and O_3 instead of H_2O. The leakage currents through the

O_3-based and the H_2O+O_3-based Al_2O_3 were more stable for the deposition temperature distribution than that through the H_2O-based Al_2O_3. The *C-V* characteristics of MIS-diodes suggested that the fixed charge in the ALD-Al_2O_3 was most reduced by using both H_2O and O_3. From *I-V* measurements on MIS-HEMTs, it was found that the MIS-HEMT with H_2O+O_3-based Al_2O_3 showed the good pinch-off characteristics with the forward bias over 6 V, and the drain leakage current was suppressed by seven orders of magnitude by the MIS-structure. These results indicate that the Al_2O_3 deposited by using both H_2O and O_3 is useful for the GaN-based MIS-devices.

Acknowledgements

We would like to thank Dr. Fujita and Dr. Wakejima for valuable discussions. This work was partly supported by the Ministry of Education, Culture, Sports, Science and Technology, the Knowledge Cluster Initiative (the Second Stage) ― Tokai Region Nanotechnology Manufacturing Cluster ―.

References

[1]T. Hashizume, S. Ootomo, T. Inagaki, and H. Hasegawa, J. Vac. Sci. Technol. B **21**, 1828 (2003).

[2]K. Park, H. Cho, E. Lee, S. Hahm, and J. Lee, J. Semicond. Tech. Sci. **5**, 107 (2005).

[3]P. D. Ye, B. Yang, K. K. Ng, J. Bude, G. D. Wilk, S. Halder, and J. C. M. Hwang, Appl. Phys. Lett. **86**, 063501 (2005).

[4]S. L. Selvaraj, and T. Egawa, Appl. Phys. Lett. **89**, 193508 (2006).

[5]T. Nanjo, T. Oichi, M. Suita, Y. Abe, and Y. Tokuda, Appl. Phys. Lett. **88**, 043503 (2006).

[6] Z. H. Liu, G. I. Ng, S. Arulkumaran, Y. K. T. Maung, K. L. Teo, S. C. Foo, V. Sahmuganathan, T. Xu, and C. H. Lee, IEEE Electron Device Lett. **31**, 96 (2010).

[7]M. Kanamura, T. Ohki, T. Kikkawa, K. Imanishi, T. Imada, A. Yamada, and N. Hara, IEEE Electron Device Lett. **31**, 189 (2010).

[8]Y. Hori, C. Mizue, and T. Hashizume, Jpn. J. Appl. Phys. **49**, 080201 (2010).

[9]J. J. Freedsman, T. Kubo, S. L. Selvaraj, and T. Egawa, Jpn. J. App. Phys. **50,** 04DF03 (2011).

[10]E. Miyazaki, Y. Goda, Shigeru Kishimoto, and T. Mizutani, Solid-State Electron. **62**, 152 (2011).

[11]C. Mizue, Y. Hori, M. Miczek, and T. Hashizume, Jpn. J. Appl. Phys. **50**, 021001 (2011).

[12]C. Liu, E. F. Chor, and L. S. Tan, Appl. Phys. Lett. **88**, 173504 (2006).

[13]S. Abermann, G. Pozzovivo, J. Kuzmik, G. Strasser, D. Pogany, J.-F. Carlin, N. Grandjean, and E. Bertagnolli, Semicond. Sci. Technol. **22**, 1272 (2007).

[14]P. Kordoš, G. Heidelberger, J. Bernát, A. Fox, M. Marso, and H. Lüth, Appl. Phys. Lett. **87**, 143501 (2005).

[15]D. Kikuta, J. P. Ao, Y. Ohno, Solid-State Electron. **50**, 316 (2006).

[16]H. Kambayashi, Y. Satoh, S. Ootomo, T. Kokawa, T. Nomura, S. Kato, and T. P. Chow, Solid-State Electron. **54**, 660 (2010).

[17]T. Hashizume, E. Alekseev, D. Pavlidis, K. S. Boutros, and J. Redwing, J. Appl. Phys. **88**, 1983 (2000).

[18]S. L. Selvaraj, T. Ito, Y. Terada, and Takashi Egawa, Appl. Phys. Lett. **90**, 173506 (2007).

[19]S. Tan, S. L. Selvaraj, and T. Egawa, Appl. Phys. Lett. **97**, 053502 (2010).

[20]J. J. Freedsman, T. Kubo, and T. Egawa, Appl. Phys. Lett. **99**, 033504, (2011).

[21]J. J. Freedsman, T. Kubo, and T. Egawa, Aip Advances, **2**, 022134 (2012).

[22]T. Oka and T. Nozawa, IEEE Electron Device Lett. **29**, 668 (2008).

[23]S. Arulkumaran, L. Z. Hong, N. G. Ing, S. L. Selvaraj, and T. Egawa, Appl. Phys. Express **2**,

031001 (2009).

[24]M. Higashiwaki, Z. Chen, R. Chu, Y. Pei, S. Keller, U. K. Mishra, N. Hirose, T. Matsui, and T. Mimura, Appl. Phys. Lett. **94**, 053513 (2009).

[25]M. Fagerlind, F. Allerstam, E. Ö. Sveinbjörnsson, N. Rorsman, A. Kakanakova-Georgieva, A. Lundskog, U. Forsberg, and E. Janzén, J. Appl. Phys. **108**, 014508 (2010).

[26]J. B. Kim, D. R. Kwon, K. Chakrabarti, C. Lee, K. Y. Oh, J. H. Lee, J. Appl. Phys. **92**, 6739 (2002).

[27]X. Liu, S. Ramanathan, A. Longdergan, A. Srivastava, E. Lee, T. E. Seidel, J. T. Barton, D. Pang, and R. G. Gordon, J. Electrochem. Soc. **152**, G213 (2005).

[28]Y. Wang, M. Dai, M. –T. Ho, L. S. Wielunski, and Y. J. Chabal, Appl. Phys. Lett. **90**, 022906 (2007).

[29]D. N. Goldstein, J. A. McCormick, and S. M. George, J. Phys. Chem. C **112**, 19530 (2008).

[30]S. Ozaki, T. Ohki, M. Kanamura, T. Imada, N. Nakamura, N. Okamoto, T. Miyajima, and T. Kikkawa, IEICE Technical Report **112**, 41 (2012).

Figure captions

FIG. 1. Schematic diagram of the ALD process using H_2O and O_3

FIG. 2. XPS (a) Al 2p and (b) O 1s spectra obtained from the ALD-Al_2O_3 surfaces.

FIG. 3. Schematic cross section view of the Al_2O_3/n-GaN MIS-diode.

FIG. 4. *I-V* characteristics of the Schottky and MIS diodes: (a)TMA+H_2O (b)TMA+O_3 (c)TMA+H_2O+O_3.

FIG. 5. *C-V* curves obtained from MIS-diodes: (a)TMA+H_2O (b)TMA+O_3 (c)TMA+H_2O+O_3.

FIG. 6. Schematic cross section view of the Al_2O_3/AlGaN/GaN MIS-HEMT.

FIG. 7. DC drain current-voltage (I_d-V_d) characteristics of the MIS-HEMTs: (a) H_2O+O_3-based Al_2O_3 (b) a typical example of the H_2O-based and the O_3-based Al_2O_3 with no pinch-off characteristics.

FIG. 8. Dependence of the drain current (I_d) and the gate leakage current (I_g) on the gate bias voltage (V_g).

TABLE I. Concentrations of H and C contents in the ALD-Al_2O_3 measured by SIMS.

Oxygen precursor	H [$\times 10^{21}$ cm^{-3}]	C [$\times 10^{19}$ cm^{-3}]
H_2O	2.8	5.5
O_3	0.7	9.6
H_2O+O_3	1.2	3.6

TABLE II. Threshold voltage of the *C*-*V* curve obtained from the MIS-diodes with Al_2O_3 deposited at 300^{o}C using H_2O, O_3, and both H_2O and O_3 as the oxygen precursors.

Precursor	H_2O	O_3	H_2O+O_3
V_{th} (V)	-1.15	-0.91	-0.63

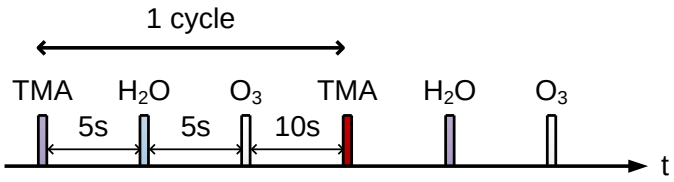

FIG. 1. Schematic diagram of the ALD process using both H_2O and O_3.

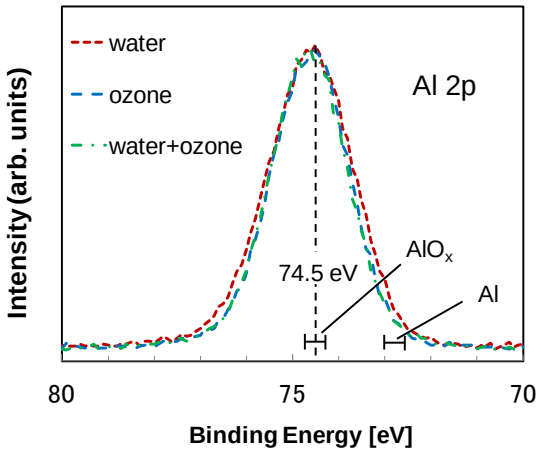

(a)

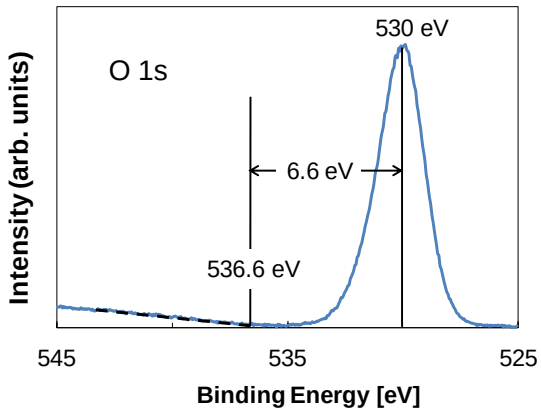

(b)

FIG. 2. XPS (a) Al 2p and (b) O 1s spectra obtained from the ALD-Al_2O_3 surfaces.

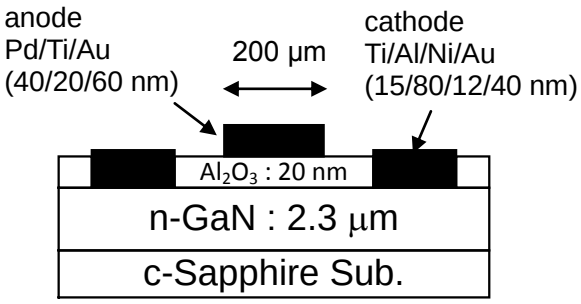

FIG. 3. Schematic cross section view of the Al_2O_3/n-GaN MIS-diode.

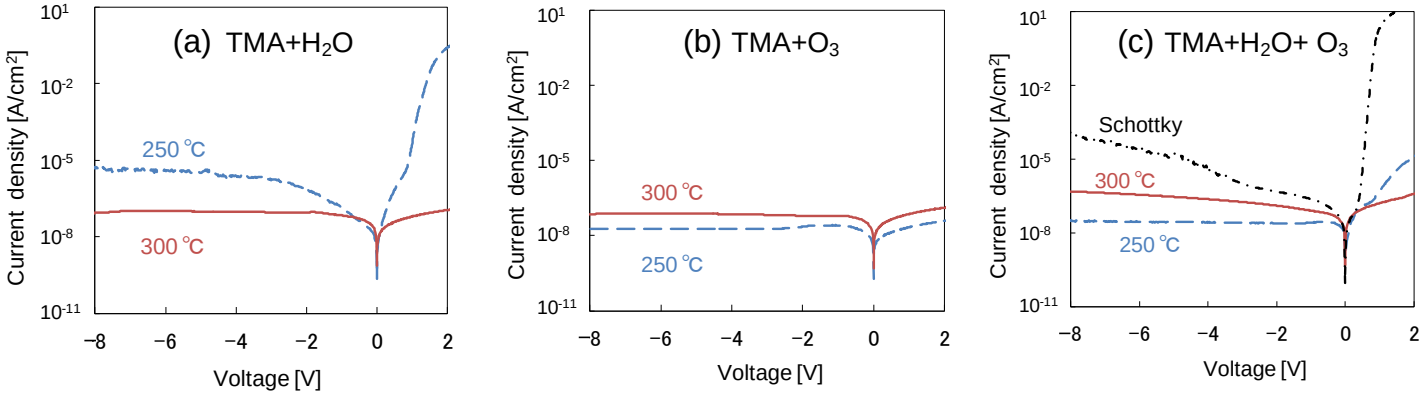

FIG. 4. *I-V* characteristics of the Schottky and MIS diodes: (a)TMA+H_2O (b)TMA+O_3 (c)TMA+H_2O+O_3.

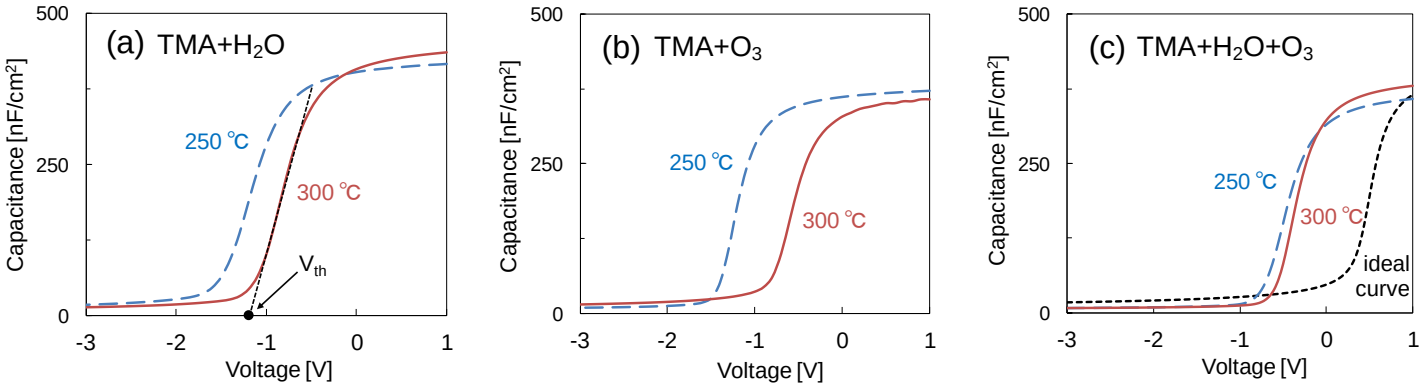

FIG. 5. *C-V* curves obtained from MIS-diodes: (a)TMA+H_2O (b)TMA+O_3 (c)TMA+H_2O+O_3.

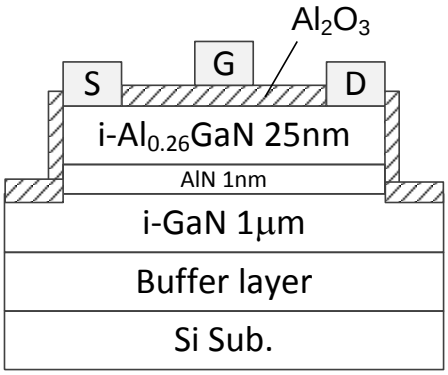

FIG. 6. Schematic cross section view of the Al_2O_3/AlGaN/GaN MIS-HEMT.

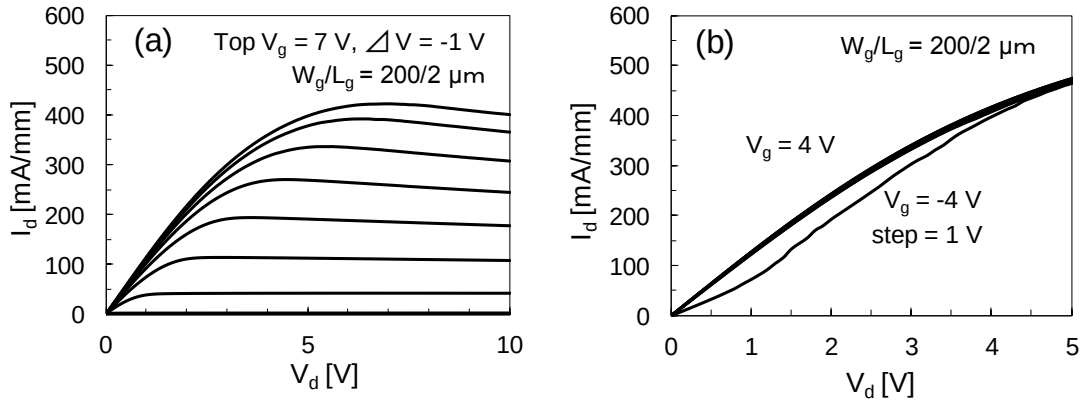

FIG. 7. DC drain current-voltage (I_d-V_d) characteristics of the MIS-HEMTs: (a) H_2O+O_3-based Al_2O_3 (b) a typical example of the H_2O-based and the O_3-based Al_2O_3 with no pinch-off characteristics.

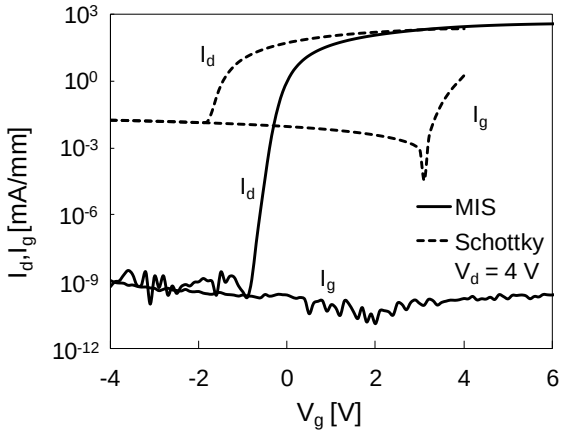

FIG. 8. Dependence of the drain current (I_d) and the gate leakage current (I_g) on the gate bias voltage (V_g).